Microstructure based strengthening model of a biocompatible WE54 alloy reinforced by SiC

M. Cabibbo, F. Průša

A large number of magnesium alloys and magnesium-based composites are nowadays used as biocompatible light metallic materials. Example of their applications include bone-tissue screws, cardiac valves, orthodontic screws and components. In this sense, the biocompatibility, durability, and corrosion resistance and blood compatibility are key factors for the full availability of magnesium based alloys in the bioengineering field. On the other hand, minimal necessary mechanical properties necessary for their potential application in such a filed were investigated in the last three decades. With this respect, not only magnesium based alloys, but also magnesium composite alloys were tested for their biocompatibility. Oxides such TiO_2, MgO, ZnO, ZrO_2, TiB_2, Al_2O_3, and also SiC showed sufficient biocompatibility and in addition, composite magnesium alloys added with such oxides or SiC are known to possess higher mechanical properties compared to their magnesium alloy counterparts. Among the different available metallurgical technologies to produce magnesium alloys, the powder metallurgy (PM) is surely one of the most promising one. With this regard, squeeze casting is one of the most reliable and cost-effective PM technique of production of magnesium based alloys and composites.
In the present work, the microstructure and mechanical properties of WE54+15vol.%SiC under various compression temperature conditions, up to 300°C, were investigated by transmission electron microscopy (TEM). Microstructure inspections revealed the formation of stable cuboid secondary phase particles, and lamellae and irregular-shaped intermetallic phases. A microstructure-based strengthening model was proposed and compared to the experimentally obtained compression stress carried out at temperatures ranging 50-to-300°C. The most effective strengthening term was found to be the one coming from the refined grain structure. A further important strengthening contribution was constituted by the secondary phase particle precipitation within the Mg-matrix.

KEYWORDS: BIOCOMPATIBLE MG-BASED ALLOYS; COMPRESSION; STRENGTHENING MODEL; TEM.

Introduction

Mg-RE (WE) alloys have driven much interest as biomedical applications due to their outstanding high strength at both room temperature and high temperatures, excellent precipitation hardening and good biocompatibility [1-3]. With this respect, commercial alloys such the WE43 and WE54 have been widely used in various structural and biomedical applications due to their good balance on performance and cost. This interest favored a number of investigations on the mechanical properties [4-6], deformation behavior [7,8], precipitation sequence [9,10] of the WE series alloys. Mg-Gd-based alloys with some Y or Nd addition exhibited

Marcello Cabibbo
DIISM / Università Politecnica delle Marche, Ancona, Italy

Filip Průša
University of Chemistry and Technology, Prague, Department of Metals and Corrosion Engineering, Technická 5, 166 28 Prague 6, Czech Republic

remarkable aging-hardening response and good ductility even after T6 treatment [11]. With this respect, Wang et al. [4] reported that over 2 wt% Gd additions significantly improved the ductility of the as-cast Mg-5Y-3Nd-0.6Zr alloy. Many researchers reported formation of particle, namely cuboid-shaped phases $Mg_{24}RE_5$ and Mg_5RE ([12] to cite but one).

The biodegradable metallic materials can be divided into three categories, such as pure metals, alloys, and composites. Commercially available AZ91D Mg alloy is considered the most suitable bio-engineering magnesium alloy, and it has been so far deeply investigated in vivo and vitro environments. On the other hand, composite materials must possess the highest level of mechanical strength, corrosion resistance and biocompatibility to be qualified as a biomaterial implant.

Ceramic-based implants were also developed due to their better mechanical performance, lack of an inflammation reaction, and optimum degradation rate. However, bio-absorbable ceramics also have fast degradation rates compared to non-absorbable ceramics. Mg-based bio-alloys are considered to absorb within the human body at an appropriate resorption rate, but they also have a problem of a fast degradation rate during tissue remodelling, which limits their applications in clinical fields [13]. For this reason, Mg-based alloys are still considered to be a good choice in the fields of tissue engineering, orthopaedics and cardiovascular stents because of their suitable mechanical properties, reasonable biodegradation and lower toxicity [13]. Researchers have developed Mg-based bio micro-composites and bio nano-composites to achieve the desired mechanical properties, optimized corrosion resistance, minimum cytotoxicity, and high biocompatibility [14-21].

Numerous opportunities and challenges still exist in developing Mg-based biodegradable composites and alloys for biomedical applications. In this sense, Mg-RE alloys (such as the WE series) provide better mechanical properties and corrosion resistance at both room and high temperatures [22].

Considerable improvement of the mechanical properties can also be achieved by reinforcement with ceramic particles or fibres. Metal matrix composites (MMCs) provide a substantial increase in strength and stiffness as well as creep resistance. The ductility of composites is significantly reduced as compared to unreinforced alloys. Bio-composites have been developed and used in tissue engineering, drug delivery, dentistry and bone implants because of their high performance. However, their low stiffness, poor mechanical properties, and inflammation issues during the implantation period have limited their use in the biomedical field [13].

The composite magnesium alloys usually contain at least two components, which are known as matrix and reinforcement. All the components of the composite must be biocompatible and nontoxic in any physiological environment. The composite material allows the combination of matrix and reinforcement properties such as sufficiently high mechanical properties (tensile strength, elastic modulus, yield strength, compression strength), corrosion resistance and biocompatibility. Thence, selection of matrix component and reinforcement component are very critical to obtain the desired properties [23,24].

In the present work a WE54 alloy added with 15%vol.SiC was tested by compression at high temperatures. Microstructure evolution was inspected by electron microscopy (TEM). The work presents a microstructure based strengthening model that was compared to the experimental compression tests carried out at temperatures ranging 50-to-300°C.

Experimental procedure

The material used in this study was a WE54 magnesium matrix composite. Commercial WE54 (Mg-5wt.%Y-4wt.%RE, mainly Nd) alloy was reinforced by 15vol.% silicon carbide particles. Composite was prepared by squeeze casting technique. In particular, a two-step squeeze casting process was followed to fabricate the WE54-SiC composite. This was constituted by a first stage of very low pressure for infiltration applied to the matrix melt, followed by melting and solidification at quite high squeezing pressure. The SiC particles were embedded in the alloy through preheating in a furnace at 400-450°C, before further maintenance at 900°C for 2 h. During squeeze casting, the applied pressure and time for infiltration were 0.4-to-0.5 MPa and 15-25 s, respectively. Then, the WE54-SiC composite alloy was melted in an electric furnace with a graphite crucible using a specific flux of inert gas protection (namely argon). The casting temperature was fixed at 750°C. For all experimen-

tal runs, the squeezing pressure after infiltration and the dwelling of the squeezing pressure were 100 MPa and 90 s, respectively.

Compression tests were carried out at temperatures between room temperature and 300°C using an INSTRON testing machine, according to ASTM E9. Cylindrical specimens of 8mm in diameter and 12 mm long were deformed at an initial strain rate of $2.8 \cdot 10^{-4}$ s^{-1}.

The microstructure was inspected by optical microscopy (OM) and by transmission electron microscopy (TEM). Thin foils for TEM were mechanically thinned down to ~100 µm, punched, and then dimpled to a thickness of ~20 µm at the center of the 3-mm disk. This was furthermore thinned to electron transparency using a precision ion polishing system (Gatan™ PIPS) with an initial tilt angle of 8°, followed by a running angle of 3°, at voltage of 4.5 V and cooled by liquid nitrogen. A Philips™ CM20® working at 200kV and equipped with a double tilt specimen holder was used. Detected secondary phase particles were identified by selected-area diffraction pattern (SAEDP).

All the here reported mean values and statistical evaluations come from at least 80 individual measurements for SiC and twin spacing. The mean values of secondary phase particles and grain size were evaluated by stereological methods (ASTM E112) and were obtained from a series of a minimum of 150 individual measurement per each experimental condition. Mean secondary phase particle diameter and SiC geometrical dimensions (length, size and thickness) were evaluated by stereological means. In particular, particle thickness was measured directly on TEM by an in-line stereo-features measurement facility.

Results and discussion

Microstructure and mechanical properties

The microstructure of the composite is reported in Figure 1. The SiC particles are not uniformly distributed in the matrix as they mostly tend to randomly cluster.

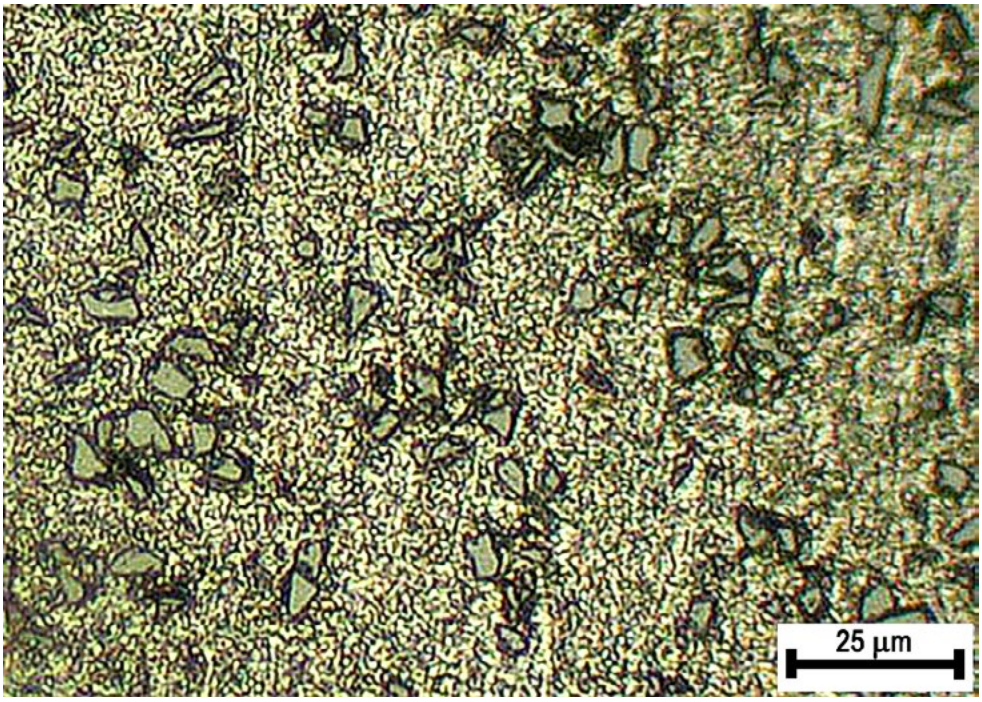

Fig.1 - Microstructure of the as-produced, undeformed WE54-15%vol.SiC composite.

The compressive true stress-strain curves at strain rate of $2.78 \times 10^{-4} s^{-1}$ and different temperatures are shown in the Figure 2 inset. Figure 2 also shows the yield stress obtained experimentally as a function of the measured alloy mean grain size, D_g. It appeared that a linear relationship between the alloy strengthening and the grain size evolution with compression temperature was identified.

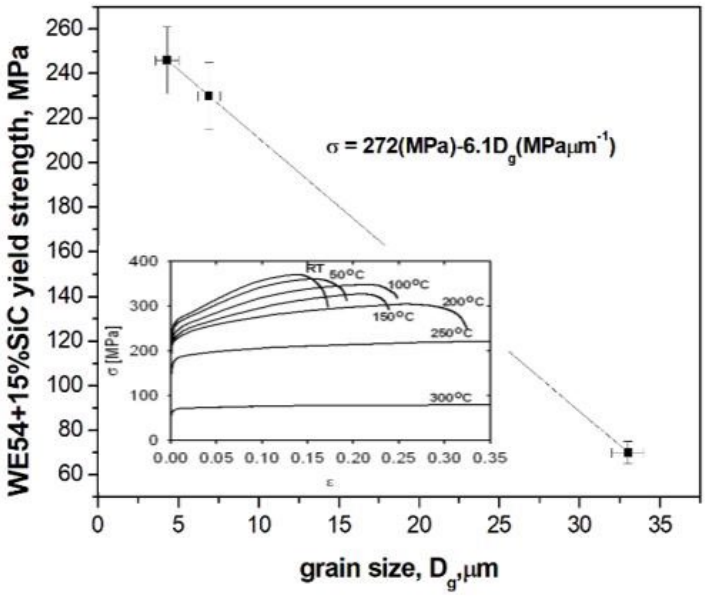

Fig.2 - Yield strength, $\sigma_{0.2}$ vs. mean grain size, D_g. Inset reports the true stress-strain curves at different compression test temperatures (room-temperature, 50, 100, 150, 200, 250, and 300°C) [25].

This was as: $\sigma_{0.2} = 272 - 6.1 \cdot D_g$, and thence in the present case, a constant strengthening ratio reduction of ~6 MPa per micron of grain size increase could be established. The temperature dependences of the characteristic stresses, the yield stress $\sigma_{0.}2$ and the ultimate stress (UTS) σ_U, are shown in Figure 3. It appears a clear influence of the test temperature on the resulting alloy strain hardening, at a test temperature beyond 200°C, as the compressive flow stress started to decrease with the temperature. In other words, the compression strength of the WE54 SiC reinforced alloy did not changed from room temperature to 200°C. This ultimately means that, according to the 90/385/EEC (active implantable medical devices directive), the compression behaviour of the present alloy is stable for the human body temperatures and for the possible local mechanical processes of working heating and cooling prior implantation.

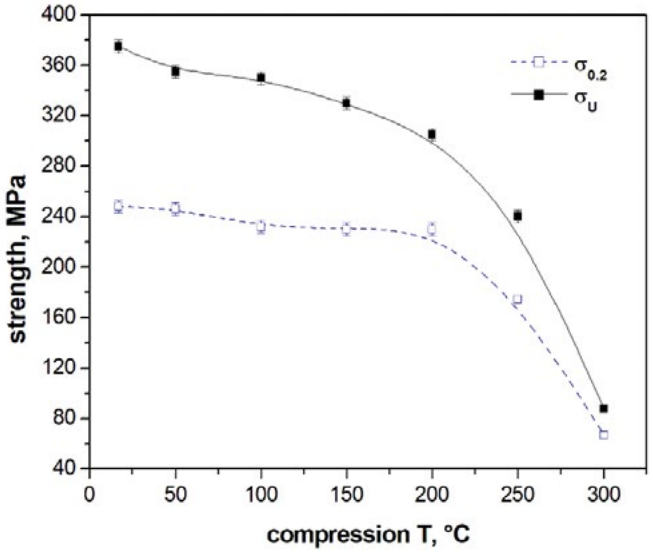

Fig.3 - Temperature dependences of the alloy strength, UTS (σ_{max}), and YS ($\sigma_{0.2}$), from room temperature (17°C) to the maximum test temperature of 300°C [25].

This interesting alloy mechanical response was accounted from a microstructure viewpoint by a systematic microstructure inspection carried out by electron microscopy (TEM).

Figure 4 reports representative TEM micrographs of the alloy microstructure at room temperature (Figure 4a), after compression test at 50°C (Figure 4b), 150° (Figure 4c), and 300°C (Figure 4d). It appeared that the microstructure remained stable up to 200°C, being quite similar to the one observed at room temperature (that is in the as-produced condition). Yet, the microstructure after the compression tests at 300°C clearly revealed a significant grain coarsening and secondary phase deterioration, that is coarsening of the reinforcing secondary phase particles. In addition, at 300°C compression test, most of the coarse secondary phase particles tend to align almost continuously at grain boundaries. This indeed correspond to a weakening morphology for the intergranular particles that can led to mechanical failure by grain decohesion. This microstructure degradation with compression temperature is ultimately believed to drive the corresponding mechanical failure of the present WE54-SiC alloy.

The microstructure inspections revealed the twin formation within the magnesium matrix. These were of nanometric scale and were found to be quite narrow and lying parallel to each other (Figure 5). Anyhow, nano-twins were detected only at testing temperature above 200°C. The important role of twinning in the deformation of hexagonal closed-packed (hcp) lattice alloys is well known. On the other hand, dislocation density plays important role in hardening mechanism in composite. With addition of the reinforcing phase, the geometrically necessary dislocations are generated to accommodate the mismatch of plastic deformation in the matrix. New dislocations arise directly in the production process due to the solidification process during preparation of the composite. A higher dislocation density in the composite material induces a higher level of internal stress. The detected higher matrix dislocation density as well as the reinforcement/matrix interfaces can provide high diffusivity paths in the composite alloy. Significant amount of dislocations were generated during compressive deformation.

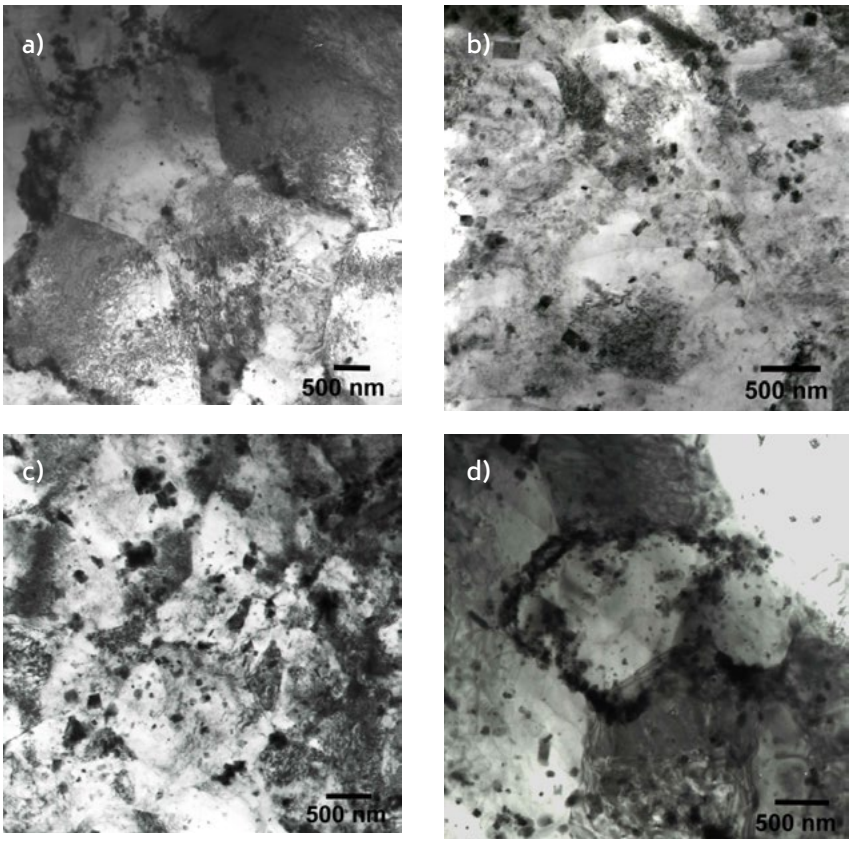

Fig.4 - Representative TEM micrographs showing the microstructure at room temperature (as-producued condition), a); after compression test at 50°C, b); 150°C, c); and at 300°C, d). Rectangular shaped secondary phase particles are $Mg_{24}Y_5$ hardening phases, according to [26].

Based on the quantitative evaluation of all the strengthening features appeared in the alloy microstructure a strengthening model was proposed. The major microstructure features contributing to the alloy strength are: grain-structure through Hall-Petch mechanism of strengthening, twinning formation, secondary phase formation and eventual coarsening, composite model of strengthening given by the SiC particles. This microstructure-based alloy strengthening model is reported in the following.

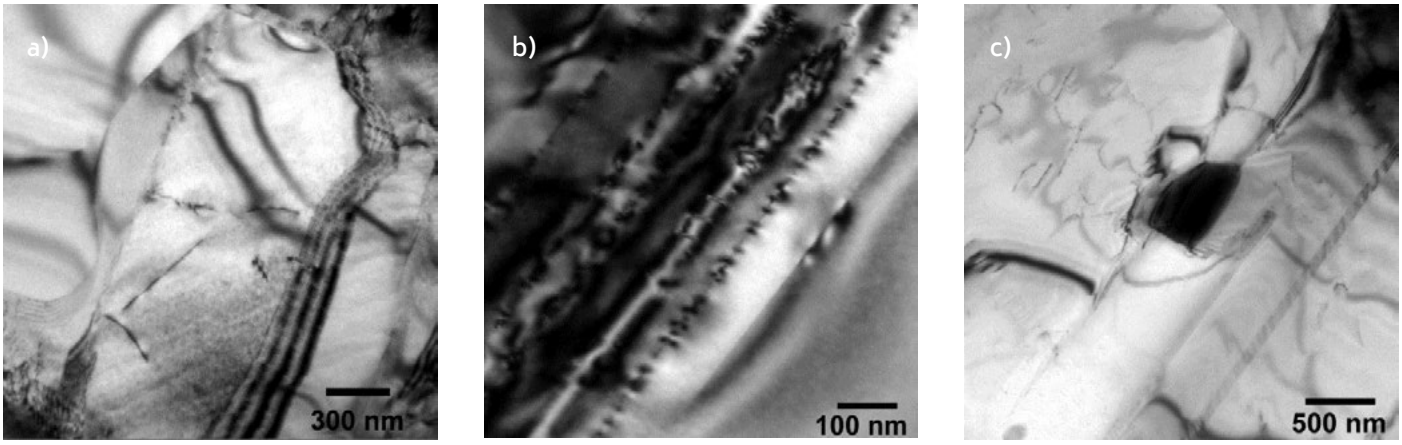

Fig.5 - Representative TEM micrographs showing the absence of nanotwins after compression at 100°C, a), the formation of nano-twins after compression test at 200°C, b), and after compression test at 300°C, c).

Microstructure-base alloy strengthening model

a. Grain size strength (Hall-Petch)

The strengthening contribution given by the grained structure of the magnesium matrix is expressed by the Hall–Petch relationship, which relates the alloy stress, $\Delta\boldsymbol{\sigma}_{HP}$, to the mean grain size, D_g, by Eq. (1), [27]:

$$\Delta\sigma_{HP} = K_{HP}\cdot(D_g)^{-0.5} \qquad (1)$$

where K_{HP} = 0.28 MPa·m$^{1/2}$ is the Hall-Petch constant [27]. This contribution varied significantly with the compression test temperature as the mean grain size increased to one-order of magnitude at the maximum test temperature of 300°C. In fact, the mean grain size varied from the minimum value obtained at the undeformed experimental condition (as-prepared), where D_g = 2.8 ± 0.6 µm, up to D_g = 4.3 ± 0.7 µm, D_g = 6.9 ± 0.7 µm, D_g = 33 ± 1 µm, after compression at 50, 150, and 300°C, respectively. These measured mean grain sizes corresponded to a Hall-Petch grain strengthening contribution of $\Delta\boldsymbol{\sigma}_{HP}$ = 165 ± 15 MPa, for the undeformed sample, and $\Delta\boldsymbol{\sigma}_{HP}$ = 135 ± 15 MPa, $\Delta\boldsymbol{\sigma}_{HP}$ = 110 ± 10 MPa, $\Delta\boldsymbol{\sigma}_{HP}$ = 50 ± 10 MPa, after compression at 50, 150, and 300°C, respectively. That is, a drastic reduction of the alloy strengthening contribution, which more than halved, occurred after compression at 300°C, respect to the strengthening contribution yield by the grained structure after compression at 150°C.

b. Twinning

Twin boundaries, $\boldsymbol{\sigma}_T$, was calculated by a Hall-Petch type relationship as follows, Eq. (2) [28]:

$$\Delta\sigma_T = V_v^{Twins}\cdot[k_{TB}\cdot(\lambda_{TB})^{-0.5}] \qquad (2)$$

Where V_v^{Twins} is the measured volume fraction of the twins, k_{TB} = 35 MPa·μm$^{1/2}$ is a Hall-Petch type constant, λ_{TB} is the average twin boundary spacing. The detection of twin formation during compression at the different temperatures was carried out by tilting the crystal as to be oriented with respect to the beam direction to show {10-12} crystallographic plane. This to highlight the twin boundary edge lying direction <10-11> | | {10-12}.

Twins were detected essentially after compression at 200°C, and not for lower testing temperatures nor in the as-prepared condition. Thus, this contribution only holds for the conditions of compression at 300°C (Figure 5). Anyhow, the volume fractions of the detected twins were quite low, being V_v^{Twins} = 2-3 vol.%. The mean twin spacing was measured as λ_{TB} = 22-to-30 nm. Thus, the twin strengthening contribution accounted for a quite low value ranging $\Delta\boldsymbol{\sigma}_T$ = 4-7 MPa. This make the twinning contribution essentially irrelevant.

c. Secondary phase particles

The strength given by the secondary phase particles is modelled by the Orowan mechanism. That is, the precipitation hardening is an effective strengthening factor not only at room temperature but also at higher temperatures, even although the secondary phase particles started to coarsen with compressive temperature. As long as these particles are within 50-80 nm in equivalent diameter these act as impenetrable particles for the sliding dislocations. Thence, gliding dislocations bows out between consecutive particles bypassing and leaving a loop around them to proceed in their sliding motion. Thence, following the pioneering works by Scattergood and Bacon, this strengthening mechanism was here modelled using Eq. (3) [29,30]:

$$\Delta\sigma_{Orowan} = \frac{T'Eb}{4\pi(1-\nu)(1+\nu)\lambda}\left[ln\left(\frac{\bar{d}}{b}\right) + B\right] \qquad \textbf{(3)}$$

where B = 0.6 for screw dislocations and 0.7 for edge dislocations, T' = 6.5 is the Taylor factor for Mg, E = 44.4 GPa is the magnesium Young's modulus, b is the Burgers vector that for Mg is 0.32 nm, ν = 0.27 is the Poisson's ratio, λ represents the average interparticle spacing, which based on ASTM E112 stereology methods $\lambda = [1.25/(d/N_V)-\pi d/4]$, with N_V the particle volume density and d the mean particle equivalent diameter [29,30]. This latter was quantitatively evaluated by TEM inspections. It resulted that the particle mean diameter, d, increased significantly form the as-produced, undeformed condition, where d = 50 ± 5 nm, to d = 90 ± 5 nm, after compression at 50°C, d = 125 ± 5 nm, after compression at 150°C, and d = 240 ± 20 nm, after the maximum test compression temperature of 300°C.

This strengthening contribution accounted for $\Delta\boldsymbol{\sigma}_{Orowan}$ = 70 ± 5 MPa, for the undeformed condition, and to $\Delta\boldsymbol{\sigma}_{Orowan}$ = 60 ± 5 MPa, $\Delta\boldsymbol{\sigma}_{Orowan}$ = 45 ± 5 MPa, and $\Delta\boldsymbol{\sigma}_{Orowan}$ = 25 ± 5 MPa, after compression at 50, 150, and 300°C, respectively.

d. SiC particle composite strength contribution

According to the shear-lag model proposed by Nardone and Prewo in [31], the composite particles do contribute to alloy reinforcement carrying a fraction of the load from the matrix. This alloy strengthening contribution strongly depends on the shape and morphology of the particles; it specifically depends on the particle aspect ratio [32]. Thus, the proposed relationship for a composite strengthened alloy is (Eq. (4a)), [31]:

$$\Delta\sigma_{LT} = V_V^{SiC}\left[1 + \frac{A(L+t)}{4L}\right]\sigma_0 + (1 - V_V^{SiC})\sigma_0 \qquad \textbf{(4a)}$$

where $\boldsymbol{\sigma 0}$ is the unreinforced matrix yield stress, Vv^{SiC} the SiC particle volume fraction, L the particle size facing the load direction, t the mean particle thickness, A = L/t the particle aspect ratio. These were directly measured on TEM. The SiC volume fraction, Vv^{SiC}, was determined using areal analysis (A_A) stereology method (ASTM E-112). For

equiaxed particles, or alternatively particles with 2D-shape close to circle, as in the present case, the Eq. (4a) reduces to Eq. (4b):

$$\Delta\sigma_{LT} = \sigma_{LT} - \sigma_0 = 0.5 V_V^{SiC} \cdot \sigma_0 \quad \textbf{(4b)}$$

A further strengthening mechanism acting in the composite WE54 alloy refers to the different thermal expansion coefficients (CTE) between the SiC particles and the magnesium matrix. This induces a dislocation density increment with the applied stress, yielding an additional strengthening contribution to the alloy. The amount of the thermal stress induced by the presence of the reinforcement depends upon the particle volume fraction, morphology, and size, and on the effective temperature change. Upon high-temperature compression, the relatively large thermal expansion coefficient between the matrix and the SiC particles creates a misfit strain at the SiC-Mg interface. Thermal stress can be partially released by the dislocation generation and accumulation in the surroundings of the reinforcement surfaces. Thus, according to [33-35] the induced extra dislocation density can be calculated as Eq. (5a):

$$\rho_T = \frac{C\varepsilon}{b} \frac{V_V^{SiC}}{(1-V_V^{SiC})} \frac{1}{t'} = \frac{C V_V^{SiC} \Delta\alpha \Delta T}{b(1-V_V^{SiC}) t'} \quad \textbf{(5a)}$$

where C = 12 for equiaxed particles, $\varepsilon = \Delta\alpha \cdot \Delta T$ is the misfit strain, ΔT is the temperature variation, $\Delta\alpha = 21 \cdot 10^{-6}\ K^{-1}$ is the difference between matrix and SiC thermal expansion, VV^{SiC} the particle volume fraction, and t' the minimum size of the SiC particles. The thermally generated dislocation density yields a strengthening contribution of (Eq. (5b)), [33,35]:

$$\Delta\sigma_T = \alpha_1 T' G b (\rho_T)^{0.5} \quad \textbf{(5b)}$$

with $\alpha 1 = 0.35$, and G = 17480 MPa is the shear modulus of Mg.

Since the average residual stress generated by the thermal expansion is of tension nature, it is actually a negative contribution to the strengthening to the magnesium composite alloy [36].

The different nature of the ceramic SiC particles respect to the metallic magnesium matrix induces geometrically necessary dislocations resulting in an additional strengthening contribution to the alloy. The resulting matrix-to-particle misfit depends on the reinforcement size and morphology [37]. The density of the geometrical necessary dislocations is given by Eq. (6a) [35,36]:

$$\rho_{GEO} = 8 V_V^{SiC} \cdot \varepsilon_p / b t' \quad \textbf{(6a)}$$

where $\varepsilon p = 0.28$ is the plastic strain. The corresponding strengthening contribution is thus (Eq. (6b)):

$$\Delta\sigma_{GEOM} = \alpha_1 T' G b (\rho_{GEOM})^{0.5} \quad \textbf{(6b)}$$

According to the statistical evaluations of all the meaningful microstructure features appearing in the Eqs. (4)-to-(6), the SiC strengthening contribution was evaluated as, Eq. (7):

$$\Delta\sigma_{SiC} = \Delta\sigma_{LT} + \Delta\sigma_T + \Delta\sigma_{GEOM} \quad \textbf{(7)}$$

Thus, $\Delta\sigma_{SiC}$ = 57 ± 3 MPa, for the undeformed condition, $\Delta\sigma_{SiC}$ = 63 ± 3 MPa, $\Delta\sigma_{SiC}$ = 115 ± 5 MPa, $\Delta\sigma_{SiC}$ = 25 ± 5 MPa, after compression at 50, 150, and 300°C, respectively. That is, the SiC strengthening contribution tended to increase steadily with the compression temperature up to 150°C, to drastically reduce, and then degrading, at 300°C.

e. Strengthening term combination

Before considering the proper combination of all the here detected strengthening terms, the individual impact on the composite alloy strengthening at the different compression temperatures was addressed. To this purpose, Figure 6 shows the trend with compression temperature of $\Delta\sigma_{HP}$, $\Delta\sigma_{Orowan}$, $\Delta\sigma_{SiC}$. It resulted that the strengthening contribution coming from the matrix (grain size, through Hall-Petch) and the one generated by the existing secondary phase particles (primarily the $Mg_{24}Y_5$ particles) steadily reduce with compression temperature. On the other hand, the contribution yield by the presence of SiC reinforcing coarser particles slightly increased from compression temperatures within 150°C, than eventually it drastically reduced from 150 to 300°C. Anyhow, the general trend with compression temperature of the overall strengthening contribution, as calculated by combining the single contributions by using Eq. (8), reported in the following, showed an almost continuous reduction up to 3-fold less from room temperature to 300°C. Figure 6 allowed identifying the $\Delta\sigma_{SiC}$ as the actual distinctive strengthening contribution with compression temperature.

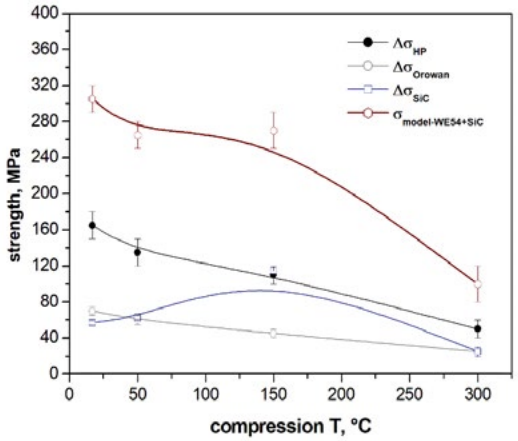

Fig.6 - Plot of the strengthening terms as calculated by Eqs. (1)-to-(6b) for $\Delta\sigma_{HP}$, $\Delta\sigma_{Orowan}$, $\Delta\sigma_{SiC}$ vs. compression temperature. The variation of σ_{model} as obtained by Eq.(8) with compression temperature is also reported for a direct comparison.

As for the overall combination of the individual strengthening contribution, according to Lilholt [38] the stress contributions acting uniformly throughout the matrix are superimposed linearly, whereas mechanisms of similar strengthening ability, which act unevenly throughout the matrix, are most suitably combined as the square root of the sum of the squares [39,40].

Thence the following model is here proposed, Eq. (8):

$$\sigma_{model} = \sigma_0 + ((\Delta\sigma_{HP} + \Delta\sigma_T + \Delta\sigma_{Orowan})^2 + \Delta\sigma_{SiC}{}^2)^{0.5} \qquad \textbf{(8)}$$

$\Delta\sigma_{SiC}$ being the strengthening contribution coming from the Sic particles as determined by linearly adding Eqs. (4)-to-(6d).

Table 1 reports the obtained results by applying the Eq. (8) to the as-prepared alloy, and the compression tested conditions at 50, 150, and 300°C.

The obtained agreement between the modelled yield strength and the experimentally measured compression strengths was of some 20% between the model and the measured values at room temperature. The difference reduced to some 10-15% for compression at 50 and 150°C, but accounted of 30% at the maximum test temperature of

300°C. In this latter case, the model overestimation is likely to be attributed to a further Orowan-like strengthening contribution that was not here taken into consideration due to a lack of experimental information. A further reason could be due to observed alloy mechanical degradation occurred at compression temperature of 300°C, which was due to an excess of grain size coarsening. This, in turns, resulted in a strength reduction of one-third respect to the value obtained for the undeformed condition. A second microstructure factor affecting the alloy mechanical degradation occurred at 300°C came from the significant reduction of the secondary phase strengthening contribution, and to a lower extent from the SiC strength contribution. The comparison between the values here obtained for the WE54-SiC composite and the ones obtained for a WE54 compressed for temperatures ranging 50-to-300°C [41] showed a significant strengthening due to the presence of SiC for test temperature up to 200°C. The mechanical degradation observed at 300°C were also observed in [41] for a WE54 SiC-unreinforced alloy.

Tab.1 - Alloy strength as obtained by applying Eq. (8) to the as-prepared alloy, and the compression tested conditions from room-temperature to 300°C.
Values coming from a WE54 alloy published by Beladi and Barnett [41] are also reported for comparison.

YS, $\sigma_{0.2}$:	undeformed	compression at 50°C	compression at 100°C	compression at 150°C	compression at 200°C	compression at 300°C
σ_{exp}, MPa	250 ± 5	245 ± 5	235 ± 5	230 ± 5	230 ± 5	70 ± 5
σ_{model}, MPa	305 ± 15	265 ± 15	-	270 ± 20	-(1)	100 ± 20
σ_{WE54}, MPa [41]	220	-	205	-	180	100

(1): The strengthening obtained for compression at 200°C are not reported here as their evaluation was jeopardized by an excess of experimental data scatter.

Conclusions

WE54 Mg-RE (RE=Y, Nd, Gd, Dy) alloy based composite was prepared by squeeze casting. Compression tests were carried out in the temperature range from room temperature up to 300°C. The stress–strain curves showed a high degree of work hardening at the lower temperatures. The most important contributions to the alloy stress were given by the matrix small grain size and by the precipitation hardening, prior of excessive coarsening upon testing at temperatures beyond 200°C. The reinforcing phase contributes to strengthening mainly through an increased dislocation density, i.e. by thermal and geometrical mismatch. It also resulted that at 300°C grain size drastically increased up to one-order of magnitude respect to the undeformed condition.

A mixed combination of the different strengthening terms was used to meet the yield stress obtained mechanically. Specifically, a linear sum of the evenly distributed strengthening terms in the matrix was quadratically combined to the contributions given by the presence of the SiC particles: $\sigma_0+((\Delta\sigma_{HP}+\Delta\sigma_T+\Delta\sigma_{Orowan})^2+\Delta\sigma_{SiC}^2)^{0.5}$. This microstructure-based model was able to describe the microstructure factors contributing to the alloy strength at the different testing temperatures.

ACKNOWLEDGEMENTS
Author wish to thank Prof. Zuzanka Trojanová for the fruitful discussion.

REFERENCES

[1] C.H. Ye, Y.F. Zheng, S.Q. Wang, T.F. Xi, Y.D. Li, In vitro corrosion and biocompatibility study of phytic acid modified WE43 magnesium alloy, Appl. Surf. Sci. 2012;258:3420-3427.

[2] F. Klocke, M. Schwade, A. Klink, A. Kopp, EDM machining capabilities of magnesium (Mg) alloy WE43 for medical applications, Procedia Eng. 2011;19:190-195.

[3] Y. Liu, S. Zheng, N. Li, H. Guo, Y. Zheng, J. Peng, Study on the in vitro degradation behavior of pure Mg and WE43 in human bile for 60 days for future usage in biliary, Mater. Lett. 2016;179:100-103.

[4] L.D. Wang, C.Y. Xing, X.L. Hou, Y.M. Wu, J.F. Sun, L.M. Wang, Microstructures and mechanical properties of as-cast Mg-5Y-3Nd-Zr-xGd (x = 0, 2 and 4 wt.%) alloys, Mater. Sci. Eng. A 2010;527:1891-1895.

[5] Y.H. Kang, H. Yan, R.S. Chen, Effects of heat treatment on the precipitates and mechanical properties of sand-cast Mg-4Y-2.3Nd-1Gd-0.6Zr magnesium alloy, Mater. Sci. Eng. A 2015;645:361-368.

[6] Y.H. Kang, X.X. Wang, N. Zhang, H. Yan, R.S. Chen, Effect of pre-deformation on microstructure and mechanical properties of WE43 magnesium alloy, Mater. Sci. Eng. A 2017;689:435-445.

[7] S.M. Zhu, J.F. Nie, Serrated flow and tensile properties of a Mg-Y-Nd alloy, Scripta Mater. 2004;50:51-55.

[8] N. Kumar, N. Dendge, R. Banerjee, R. Mishra, Effect of microstructure on the uniaxial tensile deformation behavior of Mg-4Y-3RE alloy, Mater. Sci. Eng. A 2014;590:116-131.

[9] J.F. Nie, B.C. Muddle, Characterisation of strengthening precipitate phases in a Mg-Y-Nd alloy, Acta Mater. 2000;48:1691-1703.

[10] C. Antion, P. Donnadieu, F. Perrard, A. Deschamps, C. Tassin, A. Pisch, Hardening precipitation in a Mg-4Y-3RE alloy, Acta Mater. 2003;51:5335-5348.

[11] Q. Liu, X. Ding, Y. Liu, X. Wei, Analysis on micro-structure and mechanical properties of Mg-Gd-YNd-Zr alloy and its reinforcement mechanism, J. All. Comp.d 2017;690:961-965.

[12] S.M. He, X.Q. Zeng, L.M. Peng, X. Gao, J.F. Nie, W.J. Ding, Microstructure and strengthening mechanism of high strength Mg-10Gd-2Y-0.5Zr alloy, J. All. Compd. 2007;427:316-323.

[13] M. Prakasam, J. Locs, K. Salma-Ancane, D. Loca, A. Largeteau, L. Berzina-Cimdina, Biodegradable materials and metallic implantsda review, J. Funct. Biomater. 2017;8:44-49.

[14] S. Agarwal, J. Curtin, B. Duffy, S. Jaiswal, Biodegradable magnesium alloys for orthopaedic applications: a review on corrosion, biocompatibility and surface modifications, Mater. Sci. Eng. C 2016;68:948-963.

[15] M. Pogorielov, E. Husak, A. Solodivnik, S. Zhdanov, Magnesium-based biodegradable alloys: degradation, application, and alloying elements, Interv. Med. Appl. Sci. 2017;9:27-38.

[16] J. Chen, L. Tan, X. Yu, I.P. Etim, M. Ibrahim, K. Yang, Mechanical properties of magnesium alloys for medical application: a review, J. Mech. Behav. Biomed. Mater. 2018;87:68-79.

[17] B.J.C. Luthringer, F. Feyerabend, R. Willumeit-R€omer, Magnesium-based implants: a mini-review, Magnes. Res. 2014;27:142-154.

[18] N. Li, Y. Zheng, Novel magnesium alloys developed for biomedical application: a review, J. Mater. Sci. Technol. 2013;29:489-502.

[19] L. Tan, J. Dong, J. Chen, K. Yang, Development of magnesium alloys for biomedical applications: structure, process to property relationship, Mater. Technol. 2017;1:1-9.

[20] M. Peron, J. Torgersen, F. Berto, Mg and its alloys for biomedical applications: exploring corrosion and its interplay with mecha-

nical failure, Metals (Basel) 2017;7:252-261.

[21] A. Atrens, M. Liu, N.I. Zainal Abidin, Corrosion mechanism applicable to biodegradable magnesium implants, Mater. Sci. Eng. B 2011;176:1609-1636.

[22] S.M. He, X.Q. Zeng, L.M. Peng, X. Gao, J.F. Nie, W.J. Ding, Precipitation in a Mge10Gde3Ye0.4Zr (wt.%) alloy during isothermal ageing at 250°C, J. All. Compd. 2006;421:309-313.

[23] F. Feyerabend, J. Fischer, J. Holtz, F. Witte, R. Willumeit, H. Drücker, C. Vogt, N. Hort, Evaluation of short-term effects of rare earth and other elements used in magnesium alloys on primary cells and cell lines, Acta Biomater. 2010;6:1834-1842.

[24] X. Zhang, G. Yuan, L. Mao, J. Niu, P. Fu, W. Ding, Effects of extrusion and heat treatment on the mechanical properties and biocorrosion behaviors of a Mg-Nd-Zn-Zr alloy, J. Mech. Behav. Biomed. Mater. 2012;7:77-86.

[25] Z. Száraz, Z. Trojanová, M. Cabibbo, E. Evangelista, Strengthening in a WE54 magnesium alloy containing SiC particles, Mater. Sci. Eng., A 2007;426:225-229.

[26] A.Barylski, M. Kupka, K. Aniołek, J. Rak,, The effect of precipitation hardening on the structure and mechanical and tribological properties of magnesium alloy WE54, Vacuum 2017;139:77-86.

[27] N. Hansen, Hall–Petch relation and boundary strengthening, Scripta Mater. 2004; 51:801-806.

[28] M.A. Meyers, O. Voehringer, V.A. Lubarda, The onset of twinning in metals: a constitutive description, Acta Mater. 49 (2001) 4025-4039.

[29] R.O. Scattergood, D. Bacon, The Orowan mechanism in anisotropic crystals, Philos. Mag. A 1975;31:79-198.

[30] S. Queyreau, G. Monnet, B. Devincre, Orowan strengthening and forest hardening superposition examinedby dislocation dynamics simulations, Acta Mater. 2010; 58:5586-5595.

[31] V.C. Nardone and K.M. Prewo, On the strength of discontinuous silicon carbide reinforced aluminium composites, Scripta Metall. 1986;20:43-48.

[32] M. Mabuchi and K. Higashi, Strengthening mechanisms of Mg-Si alloys, Acta Mater. 1996;11:4611-4618.

[33] R.J. Arsenault, L. Wang and C.R. Feng, Strengthening of composites due to microstructural changes in the matrix, Acta Metall. Mater. 1991;39:47-57.

[34] R.J. Arsenault and M. Taya, Thermal residual stress in metal matrix composite, Acta Metall. 1987;35:651-659.

[35] R.M. Aikin and L. Christodoulou, The role of equiaxed particles on the yield stress of composites, Scripta Metall. Mater. 1991;25:9-14.

[36] R.J. Arsenault and N. Shi, Dislocation generation due to differences between the coefficients of thermal expansion, Mater. Sci. Eng. A 1986;81:175-187.

[37] J.K. Lee, Y.Y. Earmme, H.I. Aaronson and K.C. Russell, Plastic relaxation of the transformation strain energy of a misfitting spherical precipitate: ideal plastic behaviour, Metall. Trans. A 1980;11:1837-1847.

[38] Lilholt N. Additive strengthening, deformation of multi-phase and particle containing materials. In: Hansen N, Horsewell A, Leffers T, Liohot H, editors. Roskilde, Denmark: Risø Nat. Lab; 1983. p. 381–6.

[39] Clyne T, Whithers PJ. An introduction to metal matrix composites. Cambridge: Cambridge Press; 1993.

[40] Kocks UF, Argon AR, Ashby MF. Thermodynamics and kinetics of slip. Progr. Mater. Sci. 1975;19:1-22.

[41] H. Beladi, M.R. Barnett, Influence of aging pre-treatment on the compression deformation of WE54 alloy, Mater. Sci. Eng. A 2007;452-453:306-312.